PLEASE CITE THIS ARTICLE AS DOI: 10.1063/1.5144918

Far-field Unlabelled Super-Resolution Imaging with Superoscillatory Illumination

Edward T. F. Rogers[1,2*], Shmma Quraishe[3], Katrine S. Rogers[4], Tracey A. Newman[3], Peter J. S. Smith[1,5,6], and Nikolay I. Zheludev[2,7]

[1]*Institute for Life Sciences, University of Southampton, Highfield, Southampton SO17 1BJ, UK*

[2]*Optoelectronics Research Centre and Centre for Photonic Metamaterials, University of Southampton, Highfield, Southampton SO17 1BJ, UK*

[3]*Clinical and Experimental Sciences, Faculty of Medicine, University of Southampton, Southampton, SO17 1BJ, UK*

[4]*School of Mathematics and Statistics, The Open University, Walton Hall, Milton Keynes, MK7 6AA, UK*

[5]*Biological Sciences, Faculty of Natural and Environmental Sciences, University of Southampton, Southampton, SO17 1BJ, UK*

[6]*Marine Biological Laboratory, Woods Hole, MA 02543, USA*

[7]*Centre for Disruptive Photonic Technologies, The Photonic Institute, School of Physical and Mathematical Sciences, Nanyang Technological University, 637371, Singapore*

*E.T.F.Rogers@soton.ac.uk

Abstract

Unlabelled super-resolution is the next grand challenge in imaging. Stimulated emission depletion and single-molecule microscopies have revolutionised the life sciences but are still limited by the need for reporters (labels) embedded within the sample. While the Veselago-Pendry “super-lens” using a negative-index metamaterial is a promising idea for imaging beyond the diffraction limit, there are substantial technological challenges to its realisation. Another route to far-field subwavelength focusing is using optical superoscillations: engineered interference of multiple coherent waves creating an, in principle, arbitrarily small hotspot. Here we demonstrate microscopy with superoscillatory illumination of the object and describe its underlying principles. We show that far-field images taken with superoscillatory illumination are themselves superoscillatory and hence can reveal fine structural details of the object that are lost in conventional far-field imaging. We show that the resolution of a superoscillatory microscope is determined by the size of the hotspot, rather than the bandwidth of the optical instrument. We demonstrate high-frame-rate polarisation-contrast imaging of unmodified living cells with resolution significantly exceeding that achievable with conventional instruments. This non-algorithmic, low-phototoxicity imaging technology is a powerful tool both for biological research and for super-resolution imaging of samples that do not allow labelling, such as the interior of silicon chips.

Introduction

The Abbe-Rayleigh diffraction limit of conventional optical instruments has long been a barrier to studies of microscale and nanoscale objects. The earliest attempts to overcome it recorded the evanescent field of the object: contact photography[1,2] and scanning near-field imaging (SNOM)[3–5]. Such near-field techniques can provide nanoscale resolution, but capturing evanescent fields requires a probe (or photosensitive material) to be in the immediate proximity of the object. Therefore, these techniques cannot be used to image inside cells or silicon chips,

APL Photonics ACCEPTED MANUSCRIPT
This is the author's peer reviewed, accepted manuscript. However, the online version of record will be different from this version once it has been copyedited and typeset.
PLEASE CITE THIS ARTICLE AS DOI:10.1063/1.5144918
AIP Publishing

for example. More recently, other techniques have been proposed to reconstruct and capture evanescent fields including the far-field Veselago-Pendry "super-lens", which uses a slab of negative index metamaterial as a lens to image the evanescent waves from an object on to a camera[6]. This approach, however, faces substantial technological challenges in its implementation in optics, and has not yet been developed as a practical imaging technique.

Biological super-resolution imaging is dominated by the powerful stimulated emission depletion (STED) and single-molecule localization (SML) microscopies. These far-field techniques have demonstrated the possibility of nanoscale imaging without capturing evanescent fields[7], which decay over a scale of about one wavelength away from the object. These techniques, while they have become widely used, also have their limitations. Both STED and some of the SML techniques use an intense beam to excite, deplete or bleach fluorophores in the sample. Indeed, the resolution of STED images is fundamentally linked to the intensity of the depletion beam. The damage caused by these intense beams is known as phototoxicity, as it stresses, and eventually kills, living samples. SML is also inherently slow, requiring thousands of images to be captured to build a single high-resolution image. Moreover, STED and SML require fluorescent reporters within the sample, usually achieved by genetic modification or antibody-mediated labelling with fluorescent dyes or quantum dots. Although these labels do provide a high degree of specificity, they are known to change the behaviour of the molecules or biological systems being studied[8–10] and cannot be applied to solid artificial nanostructures such as silicon chips. They also introduce a form of bias into a study: when imaging a labelled sample, you need to know in advance what part of the system displays interesting behaviour. While fluorescent imaging is easier to interpret, therefore, unlabelled imaging removes the implicit bias and exposes the native biology in all its complexity.

The other major far-field super-resolution technique is structured illumination microscopy (SIM) but it can only double the resolution of a conventional microscope[11] and requires capture of multiple images with complex post processing. It is therefore vulnerable to processing artefacts and is also conventionally applied to labelled samples. While there have been some works on unlabelled SIM[12,13], these require complex optical set-ups and algorithmic post-processing. Similar works on rotating coherent scattering microscopy[14,15] allow unlabelled imaging without post-processing but still require complex optics and remain limited to doubling the resolution of the optical system. The iSCAT technique[16,17] allows unlabelled high-resolution imaging, but only works on very clean, sparse samples, making it unsuitable for cellular biological samples. Recent work using 'traditional' SIM with superoscillatory grating illumination shows great promise[18] provided the scaling of intensity for multilobe superoscillations can be overcome. There is also a contact near-field SIM method that provides resolution beyond that of the far-field SIM technique[19]. However, in near-field SIM the object is placed in contact with the grating that provides structured illumination, and therefore is not generally suitable for bio-imaging. As with any other near-field technique, it is not comparable with the far-field superoscillatory imaging reported here.

Far-field super-resolution imaging is possible using light diffracted from a precisely engineered mask that creates extremely rapid spatial variations of electromagnetic fields in free space. These fields, known as superoscillations, have large local wave numbers (phase gradients), but more importantly can have foci much smaller than allowed by the Abbe-Rayleigh limit, as was first noted by Di Francia[20]. Superoscillatory focusing is a particular manifestation of the more general wave phenomenon of superoscillation, which was first noticed in quantum mechanics[21]. This counter-intuitive phenomenon allows any bandlimited wave to oscillate locally much faster than the highest Fourier component of the signal. The first theoretical description of optical superoscillations[22] was almost concurrent with their first observation, where subwavelength hotspots were discovered in the diffraction pattern of coherent light from a quasi-crystal array of nanoholes[23]. It was quickly realised that superoscillations could be used for super-resolution imaging without evanescent fields[24,25–27]. The mechanism of superoscillatory focusing is now well understood and is related to the formation of nanoscale vortices and energy backflow zones pinned to the focal area[28].

So far superoscillatory imaging has only been demonstrated using sparse nanostructured binary test samples[25,29] and imaging of complex unlabelled biological samples has never been achieved. Moreover, the mechanism of creating a super-resolution image with a bandlimited microscope system has not yet been explained. This raises a number of questions and challenges. How does superoscillatory illumination lead to super-resolution? Would the precise interference of multiple waves forming the superoscillatory focus be robust enough to image complex biological samples? Would light scattered from the sidebands accompanying the superoscillatory focus be sufficiently supressed to allow for accurate direct imaging without prior knowledge of the sample? Could superoscillatory imaging be combined with a contrast technique that allows study of unlabelled transparent biological samples? And finally, could a practical version of the microscope be developed which allows for video-rate imaging of live biological specimens?

To address these challenging questions, we rebuilt our superoscillatory microscope to allow optical beam scanning, rather than sample scanning, in a reflection (or epi) configuration – speeding up acquisition and allowing a petri dish of living cells to be imaged in real time. This is done by replacing the fixed binary superoscillatory lens with a spatial light modulator to shape the beam entering a high-NA objective. We also incorporate a liquid crystal polarisation controller to implement an advanced form of polarisation contrast imaging, giving high contrast even in unstained transparent biological samples (see supplementary materials for a detailed schematic of the imaging setup).

In this paper we demonstrate that superoscillatory microscopy can be efficiently used for imaging of living, unlabelled biological cells and explain the underlying mechanism of superoscillatory imaging. We constructed a practical superoscillatory microscope with which we demonstrated, for the first time, that superoscillatory imaging: 1) provides greater spatial resolution than bright-field microscopy in the same setting; 2) gives radically more information on the fine details of the object than confocal microscopy; 3) can be combined with polarisation contrast imaging for transparent objects (e.g. cells); 4) is possible at video frame rates and at low optical intensities. To illustrate these features of superoscillatory microscopy we performed resolution tests with standard test samples and conducted the first ever in-vitro, high-frame-rate super-resolution polarisation-contrast imaging of living unlabelled biological samples (mouse bone cells and neurons).

Principles of superoscillatory microscopy

A conventional microscope uses a powerful objective lens with high numerical aperture to project light scattered by the object (sample) to the image plane where it is registered. Typically, an incoherent light beam with a homogeneous profile is used to illuminate the object. The spatial resolution of a conventional microscope is limited by the focusing ability of the objective lens (its point spread function) and cannot exceed $\lambda/(2 \times \mathrm{NA})$, where λ is the wavelength of the light used for imaging and NA is the numerical aperture of the objective lens used for imaging. This is known as the Abbe-Rayleigh diffraction limit of microscopy.

In superoscillatory focusing, the interference of multiple coherent waves creates a hotspot that, in principle, can be arbitrarily small. The focus of a conventional lens with a circular aperture of finite diameter is the familiar Airy pattern, with an intense hotspot in the middle surrounded by a series of rings of increasing diameter and decreasing intensity. However, a typical superoscillatory lens creates a more complex pattern with a central hotspot surrounded by a zone of low intensity known as the "field of view". Outside this field, a broad, often high intensity, sideband, also known as the "halo", is typically observed (see inset in Figure 1). However, we will show that we can work at power levels up to 100 times smaller than standard fluorescent confocal microscopes, meaning that the halo does not cause significant phototoxicity.

Due to the presence of the halo around a superoscillatory focus, simply replacing the conventional objective lens in a widefield microscope with a superoscillatory lens is not practical for objects that are bigger than the field of view. This is because the halo will be present in the image, distorting it. The effect of the halo can, however, be mitigated by using a superoscillatory lens for structured illumination of the sample combined with confocal detection. In this configuration, a conventional lens with high numerical aperture is used as the objective lens, while the object (sample) is illuminated by a superoscillatory lens with tight focus. A small confocal aperture is used to detect only the central part of the image, thus excluding the halo. Imaging is achieved by scanning the sample relative to the focus of the superoscillatory lens. In the apparatus reported here, we implemented this configuration to improve the resolution of a conventional biological microscope with minimal modifications to the existing optics.

We now describe this configuration in more detail (see the simplified schematic of the superoscillatory microscope in Figure 1). Let the point spread functions of the illuminating superoscillatory lens, SOL, and conventional objective lens, COL, be P_{SOL} and P_{COL} respectively. The point spread function of the microscope is then $P_{\mathrm{MIC}} = P_{\mathrm{SOL}} \times P_{\mathrm{COL}}$while the microscope's response remains bandlimited to spatial frequency $\omega_{max} = 2\pi \times \mathrm{NA}/\lambda$, where NA is the average of the numerical apertures of the illuminating lens(SOL) and the imaging lens (COL), as in conventional confocal microscopy[30]. Let the object be described by function $O(\boldsymbol{r})$ that may have sub-wavelength structures: that is, $O(\boldsymbol{r})$ is not necessarily bandlimited to ω_{max}. Due to the bandwidth limitation, a conventional microscope cannot resolve fine detail beyond $\lambda/(2\mathrm{NA})$, but the superoscillatory microscope can. This is because the image $I(\boldsymbol{r}) = P_{\mathrm{MIC}} \otimes O(\boldsymbol{r})$ is also a superoscillatory function and can therefore locally oscillate much faster than ω_{max} and can contain detail finer than $\lambda/(2\mathrm{NA})$. Here the symbol $\otimes$ denotes a convolution of the point spread function of the microscope and the object.

Therefore, the main principle of superoscillatory microscopy is that superoscillatory illumination creates a superoscillatory image. We illustrate this by a trivial example of imaging a pair of narrow infinitely long slits in an opaque screen separated by 0.36λ (one-dimensional imaging). To do this we plot, in Figure 2a and 2b, hypothetical point spread functions of a superoscillatory illuminating lens $P_{\mathrm{SOL}}(x)$, a conventional imaging lens $P_{\mathrm{COL}}(x)$ and of the complete microscope system P_{MIC}. Images of the pair of slits $O(x)$ taken with conventional and superoscillatory microscopes are shown in Figure 2c and 2d, respectively. Slits separated by 0.36λ (far less than the diffraction limit of 0.5λ) are not resolved with a conventional lens and are well-resolved with superoscillatory illumination. This is possible because the image $I(x)$ itself is superoscillatory, as shown in 2d: Superoscillatory regions where $k_{\mathrm{local}} = \frac{d\varphi}{dx} > k_0$ are marked by vertical yellow lines. As is characteristic to superoscillatory functions, this image contains local spatial frequency components far higher than those in the global spectrum, as shown in 2e: the global spectrum remains bandlimited, but the local spectrum extends into regions that are not available to confocal or structured illumination microscopies.

Before going into more detail, it is instructive to compare superoscillatory imaging and STED microscopy (see Figure 3). STED (stimulated emission depletion microscopy) is a powerful technique for super-resolution microscopy. STED functions by depleting fluorescence in specific regions of the sample while leaving a central focal spot active to emit fluorescence. This focal area can be engineered by altering the properties of the depleting focal spot and the intensity of the depleting laser. In contrast, superoscillatory microscopy functions by illuminating the sample locally with a superoscillatory lens. Both are far-field super-resolution techniques that reconstruct the image non-algorithmically and without prior knowledge of the image, by scanning a hotspot across the object. While STED requires labelling of the sample with a fluorescent reporter (e.g. dye or quantum dots), superoscillatory microscopy works with unlabelled samples. STED is a nonlinear optical technique that requires intense laser radiation to deplete the fluorescence around the central focal spot, while superoscillatory microscopy is a linear imaging technique that works at any given wavelength of light and is subject only to the same signal-to-background (or contrast) requirements as any other imaging technique.

Realization of the microscope with superoscillatory illumination

Development of the superoscillatory microscope is underpinned by the design of the superoscillatory illumination. In principle, any prescribed, arbitrarily small superoscillatory focus can be constructed as a series of circular prolate spheroidal wave functions, S_i, which are bandlimited to $|k_0| \leq 2\pi/\lambda$ [24,31]. They form a complete orthogonal set over both the prescribed field of view and across the entire focal plane. However, it could happen that the chosen superoscillatory focus may only be achieved with a low intensity of the hotspot and may need a long series of wavefunctions to approximate, resulting in a complex and difficult-to-construct superoscillatory generator. Instead of targeting a pre-determined hotspot, we employed a different, simplified and more efficient strategy. Using a series of only two orthogonal circular prolate spheroidal wavefunctions (see Figure 4), we looked at which foci could be obtained by carefully balancing the amplitude coefficients of the two wavefunctions and optimizing the outcome[31].

In the superoscillatory microscope reported here, we used a superoscillatory hotspot constructed from two circular prolate spheroidal functions $E(r/\lambda) = 3.123 S_2(r/\lambda) + S_3(r/\lambda)$, where r is radial distance from the hotspot centre. Figure 4 shows sample superoscillatory hotspots that are readily achievable by tailoring the wavefront with a pair of spatial light modulators that control the intensity and phase profile of the beam incident on an objective. Here we denote the hotspot full width at half maximum as D.

The hotspot with a spot size $D = 0.4\lambda$ (equivalent to using an NA of 1.25) was used for imaging to achieve a compromise between resolution and throughput light efficiency of focusing, which affects the achievable frame rate of the instrument. In comparison, an ideal conventional lens of the same numerical aperture (NA=1.0) as the focusing lens would create a diffraction-limited focal hotspot of 0.50λ

A superoscillatory microscope can be constructed by adding a laser-based superoscillatory illumination system to a conventional microscope. We therefore used an epi-fluorescence microscope equipped with a confocal module as the platform for our superoscillatory microscope. Superoscillatory illumination of the object can be achieved either by using a static superoscillatory lens[32,33] or by shaping the input wavefront with spatial light modulators[29,34–36]. The second approach, used in our instrument, has the advantages of allowing fast and easy reconfiguration of the hotspot, and adaptive correction of instrumental imperfections in the optical path[37], as well as enabling high-speed beam scanning. A sequence of two spatial light modulators allowed the conversion of the input laser beam (λ=488nm, Newport Excelsior ONE) with a Gaussian profile into a carefully balanced superposition of two circular prolate

APL Photonics ACCEPTED MANUSCRIPT

spheroidal wave functions to achieve the superoscillatory focus. A microscope objective with effective NA=1.0 was used to focus the beam into a superoscillatory hotspot on the living cell through a cover slip, which was scanned using a pair of mirrors. Light scattered from the object was imaged by the same objective onto a pinhole and photomultiplier tube, the signal from which was used to record the image. The entire system, including spatial light modulators, scanning mirrors and detector, was computer controlled. We have achieved superoscillatory imaging at a rate of 30 frames per second over a 512x512 pixel image.

To deliver sufficient image contrast from transparent fixed or living biological samples, we combined superoscillatory and polarisation contrast imaging[38,39]. Polarisation microscopy in biological applications depends on local anisotropy and, since the earliest work by W.J. Schmidt and S. Inoue[40], has been used to illustrate the dynamic complexity of cellular substructures in living systems [41–46]. Four images were taken of the sample with relative polarisation azimuth of the illuminating beam at 0°, 45°, 90° and 135°. By combining these images computationally, we can recover the local anisotropy of the sample at each pixel, represented by the differences in reflection, R, and the incident polarisation angle, φ, at which maximum light is reflected (see formulae in the Supplementary Materials). For display in a colour figure (Figures 5 b/iii; 6 b, c; 7 a, b), information on R and φ is encoded such that brightness represents magnitude of anisotropy R (on a linear scale normalised to the maximum anisotropy in the sample) and hue encodes the polarisation azimuth φ. Thus, isotropic regions (those outside the sample for instance) are dark, where strongly anisotropic (highly structured) regions are bright. Polarisation in the regions encoded in a particular hue (say, red) is aligned in the same direction.

Imaging with the superoscillatory microscope

We tested the microscope resolution using a Siemens star, a recommended test pattern for super-resolution imaging[47] (Figure 5). The superoscillatory microscope provides better transfer of the high-frequency components of the bandlimited spectrum. This helps the visibility of fine structures in the Siemens star. With this type of sample, the key metric is how close to the centre we can faithfully image. We see significantly increased sharpness in the superoscillatory image compared to the widefield image, particularly around the middle (2.9μm) dashed yellow circle in (i) – corresponding to a grating pitch of 250nm as determined by the grating geometry.

To quantify the image improvement, we measure the fringe visibility around the circumference of a circle of decreasing radius in the image. As the radius decreases, the pitch (or distance between grating lines) of the grating decreases and hence the spatial frequency increases. Figure 5 c shows the variation of visibility with spatial frequency (lower scale) and effective pitch of the grating (upper scale) for simulated (dotted lines) and experimental (dashed lines) images. Simulation and experiment show very similar trends. The resolution is defined as the point at which the signal drops below a chosen threshold. We choose the threshold visually from the Siemens star images (Figure 5 a and b) by determining how far into the centre the spokes are visible. We select the threshold as 0.07 units (black dotted line in panel c) and use this to determine the resolution in spatial frequency (lower scale) and nm (upper scale) for all plots. These resolutions are marked with vertical dotted/dashed lines in panel c and circles in (ii) and (iii). Superoscillatory microscope images achieve a perceived resolution of 235 [217] nm in experiment [simulation] which is a factor of 1.5 improvement over the 341 [311] nm resolution offered by brightfield imaging. Here we note that the achieved resolution of 228nm is close to the size of the illuminating superoscillatory hotspot $D = 0.4\lambda = 195\text{nm}$. The size of the hotspot is set experimentally and can be made smaller at the expense of transferring more energy to the sidebands. This spot size was chosen to demonstrate the super-resolution capability while maintaining high signal levels. In this set-up, smaller spot

APL Photonics ACCEPTED MANUSCRIPT

This is the author's peer reviewed, accepted manuscript. However, the online version of record will be different from this version once it has been copyedited and typeset.
PLEASE CITE THIS ARTICLE AS DOI:10.1063/1.5144918

AIP Publishing

sizes would reduce the signal and hence the achievable frame rate, but this can be easily compensated with a higher laser power than the 100µW used here while staying well below the 1-10mW used in fluorescent confocal imaging.

We have also demonstrated imaging of biological samples. Imaging of biological samples has many challenges, beyond just achieving good lateral resolution. Intense light can easily damage biological samples, and hence it is preferable to work at low illumination intensities. Superoscillatory imaging is therefore well placed, in contrast with STED imaging, for example, which inherently requires intensities above the saturation intensity of the fluorophore in use to achieve high resolutions. Indeed, in principle, superoscillatory focusing and imaging can be performed at arbitrarily low intensity levels, down to the level of single photon illumination[48]. Note also that the lack of an absorbing reporter in the sample significantly reduces any phototoxic effects of the laser illumination, meaning that even in systems with a significant proportion of energy in the sidebands, total photon dose absorbed by the sample is much reduced. Live bioimaging also demands rapid image acquisition to capture dynamic processes. Our superoscillatory microscope uses scanning mechanisms similar to that of conventional confocal imaging and capture rates of up to 30 frames per second. However, bioimaging of transparent objects such as cells is complicated by a lack of intensity contrast, while optical anisotropy commonly occurs through molecular structuring[41,42]. To improve imaging of such samples we use polarized superoscillatory illumination to add anisotropy contrast to superoscillatory images and remove the need for fluorescent labelling, as described above.

To demonstrate biological imaging, we image both relatively well-known structures, where resolution measures can be taken (Figure 6) and more complex living cellular systems (Figure 7) with a range of scales and morphologies. We provide exemplar still images in this paper: equivalent videos of the live systems can be found in the Supplementary Materials. Figure 6b shows a section of a single living neuronal process (panel a – conventional brightfield: primary culture of a hippocampal neuron), the long thin outgrowth from the neuron used to form network connections in the brain. In panel b (superoscillatory polarisation image), the two sides of the process are clearly resolved. The widths of the two lines measured as the full width at half maximum of a profile of the magnitude of anisotropy, are 157 nm ($\lambda/3.1$) and 168 nm ($\lambda/2.9$), considerably below 298nm, the diffraction limit of a conventional lens with the same NA (equal to 1) as our objective. Note also the very clear isotropic gap between the two sides of the process (panel b), showing a nanoscale change in the polarisation structure of the process. Panel c shows an image of a similar live neuronal process, with profiles through the coloured lines shown in panel d. Knowledge about the structure and dynamics of these neuronal processes are important in understanding the changes that occur in neurodegenerative conditions such as Alzheimer's disease and dementia. It should be noted that interpreting these images is not simple. The complex interaction of polarised light reflected from the boundaries of a highly inhomogeneous and anisotropic medium is complex, and is further complicated by interference with light reflected from the interface between the coverslip and the sample. For example, the change in polarisation direction (denoted by colour) between the sides of the axonal process in Figure 7 b is counter-intuitive and requires further investigation. While the microscope does give quantitative polarisation measurements of simple samples (as seen in figure 5), quantitative analysis of the anisotropy of biological samples, therefore, remains an open question, and would require further experimentation with simplified biological preparations. Having said this, polarisation remains a powerful tool for obtaining contrast in unlabelled samples, and has been shown to reveal interesting and biologically important information in similar preparations[49,50].

APL Photonics ACCEPTED MANUSCRIPT
This is the author's peer reviewed, accepted manuscript. However, the online version of record will be different from this version once it has been copyedited and typeset.
PLEASE CITE THIS ARTICLE AS DOI:10.1063/1.5144918
AIP Publishing

As a demonstration of further applications of the superoscillatory microscope we have imaged different cell types using the different modalities of our instrument (Figure 7). We have opted to study morphologically and ultrastructurally distinct cells of the nervous and skeletal systems as they are routinely investigated using conventional microscopy. Figure 7 a shows a live image taken by the superoscillatory microscope of an unlabelled MG63 cell (human bone cell line), with zoom-ins detailing a single filopodium: an actin-filled protrusion used by the cell in its migration across the coverslip. Cancer cells are known to have modified migratory behaviour, making study of these systems highly relevant. Panel b shows the growth cone of an unlabelled mouse hippocampal neuron, where the characteristic fan shape is seen in great detail. The growth cone, at the leading tip of growing neuronal connection, determines how neurons form the networks that underlie functionality of the brain. Both the images of the bone cell and the growth cone exhibit a complexity from subcellular anisotropic structures. Such a complexity is to be expected from earlier Polscope [34,35] studies as well as 3D electron tomography of fixed cells, such as the immortalized pancreatic beta cell line, HIT-T15[51].

In Figure 7 c we show a non-polarised superoscillatory reflection image of an unlabelled MG63 cell taken from a real-time video captured at 3 frames per second. This also shows filopodia and superoscillatory spatial resolution but not the super-resolution of the anisotropic complexity exhibited in panel a. It does demonstrate an additional mode of the superoscillatory microscope. This type of reflection-mode imaging goes beyond conventional resolution, which is very helpful in understanding the adhesion of cells to surfaces, which are key regulators of cell behaviour and inter-cell signalling.

As well as the novel polarisation-contrast imaging, the fact that we have developed our microscope on a conventional confocal platform allows simultaneous capture of fluorescent images, enabling the correlative microscopy that is becoming increasingly important in biological imaging. Figure 7 d shows a two-colour image where the green channel shows the magnitude of anisotropy with superoscillatory resolution and the red channel shows diffraction-limited confocal fluorescence from MitoTracker (a live-cell-compatible mitochondrial reporter). Images like this allow us to unpick the detail of the polarisation coding and eventually determine which biological structures are causing the polarisation signal, giving insight into cellular dynamics.

Collectively, these images show living cells in real time with minimal perturbation. They demonstrate how the superoscillatory instrument may be applied across a range of important biomedical areas, revealing new information in critical areas of study, such as the biomechanics of cancer and the mechanisms of neuronal dysfunction.

Conclusions

Our paper reports new label-free biological imaging that beats in resolution all other label-free techniques. We provide, for the first time, a mathematical description of a super-resolution imaging apparatus exploiting superoscillatory illumination of the sample with confocal detection of the image formed by a conventional lens. We show that super-resolution can be achieved by this bandlimited optical instrument because the obtained image is a two-dimensional superoscillatory function. Hence, the spatial resolution of our microscope is set by the size of the superoscillatory hotspot and can break the Abbe-Rayleigh diffraction limit. We demonstrate that the local spatial resolution of a superoscillatory imaging system depends on the size of superoscillatory hotspot that, in principle, can be arbitrarily small. We outline the construction of an imaging apparatus that is a modification of a conventional commercial optical microscope where conventional illumination is replaced with beam shaping optics

APL Photonics ACCEPTED MANUSCRIPT

This is the author's peer reviewed, accepted manuscript. However, the online version of record will be different from this version once it has been copyedited and typeset.
PLEASE CITE THIS ARTICLE AS DOI:10.1063/1.5144918

AIP Publishing

based on spatial light modulators. We show that our microscope can image minimally-perturbed living cells with super-resolution at video frame rates, allowing new insights into their biological function. Finally, we show the potential for correlative microscopy where super-resolution polarised microscopy can be combined with standard fluorescence-based confocal detection, promising an avenue to identify the biological structures behind the complex anisotropic features recorded.

Superoscillatory polarisation contrast imaging is a new approach in the fundamentally important quest for ever higher resolution biological imaging with minimal perturbation of the sample. Using standard Siemens Star resolution test patterns, we have demonstrated a resolution close to the size of the illuminating superoscillatory hotspot and a factor of 1.5 better than that of bright-field imaging. Moreover, we show that this resolution can be translated into biological samples using laser powers 10-100 times lower than fluorescent confocal microscopes. The capabilities of our microscope have been demonstrated on different cell types in different microscopy modalities, showing that it can work on a range of cell morphologies and scales and in a range of applications. The unique combination of advantages: unlabelled super-resolution, simple implementation, no *a priori* knowledge of the sample and low phototoxicity, makes imaging with superoscillatory illumination a powerful tool for biological research and super-resolution imaging of samples that do not allow labelling, such as silicon chips.

Supplementary material

See supplementary material for a detailed description of the microscope construction, a comparison between confocal and superoscillatory imaging, and extended captions for the videos in Figure 7.

Acknowledgements

This research was supported by the Wessex Medical Trust Research (grant WM03), University of Southampton: Institute for Life Sciences and Enterprise Fund, the UK's Engineering and Physical Sciences Research Council (grant EP/M009122/1), and Singapore Ministry of Education Academic Research Funds Tier 3 MOE2016-T3-1-006 (S).

The authors would like to thank Guanghui Yuan for numerous fruitful discussions; Alexander Buchnev and Jun Yu Ou for fabrication of the test masks; Grace Hallinan, Aleks Pitera and Katrin Deinhardt for assistance with the neuronal cultures; Rudolf Oldenbourg for fruitful discussions; Mark Willet of the Microscopy Facility in Biological Sciences at the University of Southampton) for the matched fluorescent and DIC photos of HeLa cells used in Figure 3.

Author contributions

ETFR and NIZ conceived the superoscillatory microscope concept and developed the methodology of superoscillatory imaging to achieve super-resolution. PJSS and ETFR developed the idea of polarisation-contrast superoscillatory microscopy. ETFR built the microscope and developed the associated software, captured the data, processed the images, and carried out the imaging simulations. KSR and ETFR designed the superoscillatory spots. SQ and TAN developed the live-cell culture techniques for superoscillatory imaging. TAN supervised the cell-culture development. TAN and PJSS selected the biological targets. ETFR and NIZ wrote the manuscript. All authors discussed the results extensively and edited the manuscript. PJSS and NIZ supervised and coordinated the work.

Competing interests

The authors declare no competing financial interests.

Data Availability Statement

The data underlying this paper is available from the University of Southampton ePrints repository at http://doi.org/10.5258/SOTON/D0598. Matlab code for processing and analysing the data is available on reasonable request from E.T.F.Rogers@soton.ac.uk.

References

[1] S. Chou, P. Krauss, and P. Renstrom, Appl. Phys. Lett. **67**, 3114 (1995).

[2] S.J. McNab and R.J. Blaikie, Appl. Opt. **39**, 20 (2000).

[3] E.H. Synge, Philos. Mag. **6**, 356 (1928).

[4] D.W. Pohl, W. Denk, and M. Lanz, Appl. Phys. Lett. **44**, 651 (1984).

[5] A. Lewis, M. Isaacson, A. Harootunian, and A. Muray, Ultramicroscopy **13**, 227 (1984).

[6] J.B. Pendry, Phys. Rev. Lett. **85**, 3966 (2000).

[7] S.W. Hell, S.J. Sahl, M. Bates, X. Zhuang, R. Heintzmann, M.J. Booth, J. Bewersdorf, G. Shtengel, H. Hess, P. Tinnefeld, A. Honigmann, S. Jakobs, I. Testa, L. Cognet, B. Lounis, H. Ewers, S.J. Davis, C. Eggeling, D. Klenerman, K.I. Willig, G. Vicidomini, M. Castello, A. Diaspro, and T. Cordes, J. Phys. D. Appl. Phys. **48**, 443001 (2015).

[8] R.C.G. Smith, P.S. Stumpf, S.J. Ridden, A. Sim, S. Filippi, H.A. Harrington, and B.D. MacArthur, Biophys. J. **112**, 2641 (2017).

[9] M.T. Swulius and G.J. Jensen, J. Bacteriol. **194**, 6382 (2012).

[10] U. Schnell, F. Dijk, K.A. Sjollema, and B.N.G. Giepmans, Nat. Methods **9**, 152 (2012).

[11] M.G. Gustafsson, J. Microsc. **198**, 82 (2000).

[12] S. Chowdhury, A.-H. Dhalla, and J. Izatt, Biomed. Opt. Express **3**, 1841 (2012).

[13] B. Littleton, K. Lai, D. Longstaff, V. Sarafis, P. Munroe, N. Heckenberg, and H.

Rubinsztein-Dunlop, Micron **38**, 150 (2007).

[14] D. Ruh, J. Mutschler, M. Michelbach, and A. Rohrbach, Optica **5**, 1371 (2018).

[15] F. Jünger, P. V. Olshausen, and A. Rohrbach, Sci. Rep. **6**, 1 (2016).

[16] M. Piliarik and V. Sandoghdar, Nat. Commun. **5**, 4495 (2014).

[17] J. Ortega-Arroyo and P. Kukura, Phys. Chem. Chem. Phys. **14**, 15625 (2012).

[18] N. Shapira, Z. Deng, R. Remez, D. Singh, E. Katzav, and A. Arie, Opt. Express **27**, 34530 (2019).

[19] J.M. Guerra, Appl. Phys. Lett. **66**, 3555 (1995).

[20] G.T. Di Francia, Nuovo Cim. **9**, 426 (1952).

[21] Y. Aharonov, D. Albert, and L. Vaidman, Phys. Rev. Lett. **60**, 1351 (1988).

[22] M. V. Berry and S. Popescu, J. Phys. A. Math. Gen. **39**, 6965 (2006).

[23] F.M. Huang, N.I. Zheludev, Y. Chen, and F. Javier Garcia de Abajo, Appl. Phys. Lett. **90**, 091119 (2007).

[24] F.M. Huang and N.I. Zheludev, Nano Lett. **9**, 1249 (2009).

[25] E.T.F. Rogers, J. Lindberg, T. Roy, S. Savo, J.E. Chad, M.R. Dennis, and N.I. Zheludev, Nat. Mater. **11**, 432 (2012).

[26] A.M.H. Wong and G. V. Eleftheriades, Sci. Rep. **3**, 1715 (2013).

[27] A.M.H. Wong and G. V. Eleftheriades, Phys. Rev. B **95**, (2017).

[28] G.H. Yuan, E.T.F. Rogers, and N.I. Zheludev, Light Sci. Appl. In press (2018).

[29] S. Kosmeier, M. Mazilu, J. Baumgartl, and K. Dholakia, J. Opt. **13**, 105707 (2011).

[30] T. Wilson and C.J.R. Sheppard, *Theory and Practice of Scanning Optical Microscopy* (Academic Press (London) Ltd, London, UK, 1984).

[31] K.S. Rogers, K.N. Bourdakos, G.H. Yuan, S. Mahajan, and E.T.F. Rogers, Opt. Express **26**, 8095 (2018).

[32] E.T.F. Rogers, S. Savo, J. Lindberg, T. Roy, M.R. Dennis, and N.I. Zheludev, Appl.

APL Photonics ACCEPTED MANUSCRIPT

Phys. Lett. **102**, 031108 (2013).

[33] G.H. Yuan, E.T.F. Rogers, T. Roy, and N.I. Zheludev, Opt. Express **22**, 6428 (2014).

[34] J. Baumgartl, S. Kosmeier, M. Mazilu, E.T.F. Rogers, N.I. Zheludev, and K. Dholakia, Appl. Phys. Lett. **98**, 181109 (2011).

[35] M.A.A. Neil, R. Juškaitis, T. Wilson, Z.J. Laczik, and V. Sarafis, Opt. Lett. **25**, 245 (2000).

[36] M. Martinez-Corral, P. Andres, C.J. Zapata-Rodriguez, and C.J.R. Sheppard, Optik (Stuttg). **107**, 145 (1998).

[37] M.J. Booth, Light Sci. Appl. **3**, e165 (2014).

[38] A. Le Gratiet, M. Dubreuil, S. Rivet, and Y. Le Grand, Opt. Lett. **41**, 4336 (2016).

[39] S.B. Mehta, M. Shribak, and R. Oldenbourg, J. Opt. **15**, 094007 (2013).

[40] K. Baumann, Nat. Cell Biol. **11**, S10 (2009).

[41] K. Katoh, K. Hammar, P.J.S. Smith, and R. Oldenbourg, Proc. Natl. Acad. Sci. U. S. A. **96**, 7928 (1999).

[42] K. Katoh, K. Hammar, P.J.S. Smith, and R. Oldenbourg, Mol. Biol. Cell **10**, 197 (1999).

[43] N.M. Kalwani, C.A. Ong, A.C. Lysaght, S.J. Haward, G.H. McKinley, and K.M. Stankovic, J. Biomed. Opt. **18**, 026021 (2013).

[44] J.C.M. Low, T.J. Ober, G.H. McKinley, and K.M. Stankovic, Biomed. Opt. Express **6**, 599 (2015).

[45] E.J. Jáuregui, O. Akil, C. Acevedo, F. Hall-Glenn, B.S. Tsai, H.A. Bale, E. Liebenberg, M.B. Humphrey, R.O. Ritchie, L.R. Lustig, and T. Alliston, Bone **89**, 7 (2016).

[46] C.B. Raub, S.C. Hsu, E.F. Chan, R. Shirazi, A.C. Chen, E. Chnari, E.J. Semler, and R.L. Sah, Osteoarthr. Cartil. **21**, 860 (2013).

[47] R. Horstmeyer, R. Heintzmann, G. Popescu, L. Waller, and C. Yang, Nat. Photonics **10**, 68 (2016).

APL Photonics ACCEPTED MANUSCRIPT

This is the author's peer reviewed, accepted manuscript. However, the online version of record will be different from this version once it has been copyedited and typeset.
PLEASE CITE THIS ARTICLE AS DOI:10.1063/1.5144918

AIP Publishing

[48] G.H. Yuan, S. Vezzoli, C. Altuzarra, E.T.F. Rogers, C. Couteau, C. Soci, and N.I. Zheludev, Light Sci. Appl. **5**, e16127 (2016).

[49] G. Danuser and R. Oldenbourg, Biophys. J. **79**, 191 (2000).

[50] R. Oldenbourg, K. Katoh, and G. Danuser, Biophys. J. **78**, 1176 (2000).

[51] B.J. Marsh, D.N. Mastronarde, K.F. Buttle, K.E. Howell, and J.R. McIntosh, Proc. Natl. Acad. Sci. **98**, 2399 (2001).

Figure captions

Figure 1: **Principles of microscopy with superoscillatory illumination.** Figure shows a simplified layout of the microscope in transmission mode (for the layout of the epi version of the instrument, see details in the Supplementary Materials). Inset in the upper right corner shows the structure of a superoscillatory hotspot.

Figure 2: **Superoscillatory illumination creates superoscillatory images with sub-diffraction features.** a) Point spread functions of the illuminating superoscillatory lens P_{SOL} (blue solid line) and of the conventional imaging lens P_{COL} (orange dashed line) used in the imaging apparatus; b) Combined point spread function P_{MIC} of the superoscillatory microscope; c) Test object – two slits in an opaque screen – $O(\boldsymbol{x})$ (black solid line) and its brightfield image $P_{\mathrm{COL}} \otimes O(x)$ taken with a conventional lens (orange dashed line). Slits are not resolved with a conventional lens; d) Superoscillatory image of the slits $P_{\mathrm{MIC}} \otimes O(\boldsymbol{x})$ resolves the slits (blue line). Superoscillatory regions with fast variation of the phase are marked by vertical yellow lines. e) Spatial spectra (log scale) of the entire image $P_{\mathrm{MIC}} \otimes O(\boldsymbol{x})$ (blue solid line) and its central feature (orange dashed line). Note that the spectrum of the entire image is band limited to double the Abbe-Rayleigh limit, as it is in confocal imaging. The green region highlights the region beyond the conventional band limit of confocal imaging.

Figure 3: **Microscopy with superoscillatory illumination vs STED microscopy.** a) In STED microscopy, a sample is imaged by collecting fluorescence from a small sub-wavelength spot of the sample, which must contain a fluorescent label. The fluorescent spot (bright area in the centre of grey disk) is surrounded by a larger dark area where fluorescence is depleted by intense laser radiation (orange disk). b) In superoscillatory imaging, a sample is imaged by collecting light scattered from a small area illuminated by light focused into a sub-wavelength superoscillatory spot (bright spot in the centre of a bigger halo).

Figure 4: **Engineering of superoscillatory hotspots.** A range of superoscillatory spots showing the flexibility of the design algorithm with varying spot size. The superoscillatory spot used in the biological imaging is highlighted in green. Below each spot is the equation describing the construction of the spot from circular prolate spheroidal wavefunctions.

Figure 5: **Imaging the Siemens star**. Panels a and b show images of a 36-sector binary Siemens star test object: (a/i) test sample design and (b/i) SEM images of the sample (40nm chromium film on glass substrate structured with focused ion beam); (a/ii) simulated and (b/ii) experimental brightfield image with a conventional lens; (a/iii) simulated and (b/iii) experimental superoscillatory image with polarisation contrast. See text for a description of the false-colour scheme used in c/iii. Yellow dashed circles in (i) are for scale and have diameters of 1.1, 2.9 and 4.6 µm. Circles in (ii) and (iii) show resolution limits with line styles matching panel c. Panel c shows spatial spectra of conventional brightfield images, and superoscillatory images of the Siemens star (dashed lines – experiment, dotted lines – computer simulation; vertical dashed [dotted] lines show the limits of resolution in experiment [simulation]). The resolution threshold is shown by the black dotted line. Note the radical increase of high-frequency components in the superoscillatory spectrum, in contrast to brightfield, making fine details of the image visible.

Figure 6**: Superoscillatory imaging of biological structures.** Conventional brightfield image of a living neuronal process (a) and superoscillatory image of the region within the yellow box (b). See text for a description of the

APL Photonics ACCEPTED MANUSCRIPT

false-colour scheme used in b and d. Panel a is deliberately slightly defocused to provide brightfield contrast in the transparent axon sample. Panel c: Superoscillatory image of a live neuronal segment. Panel d: Profiles along the lines shown in panel c.

Figure 7: **Different modalities of superoscillatory imaging of living cells.** (a) Superoscillatory polarisation-contrast image of unlabelled MG63 cell. Inset shows an enlargement of a filipodium. (b) Superoscillatory polarisation-contrast image of a growth cone in an unlabelled mouse neuron. See text for a description of the false-colour scheme used in a and b. (c) Non-polarised reflection mode superoscillatory image of an unlabelled MG63 cell. (d) Superoscillatory image (magnitude only, green channel) combined with a confocal fluorescently labelled image (MitoTracker red, red channel) of an MG63 cell. (Multimedia view - See supplementary information for details of video.)

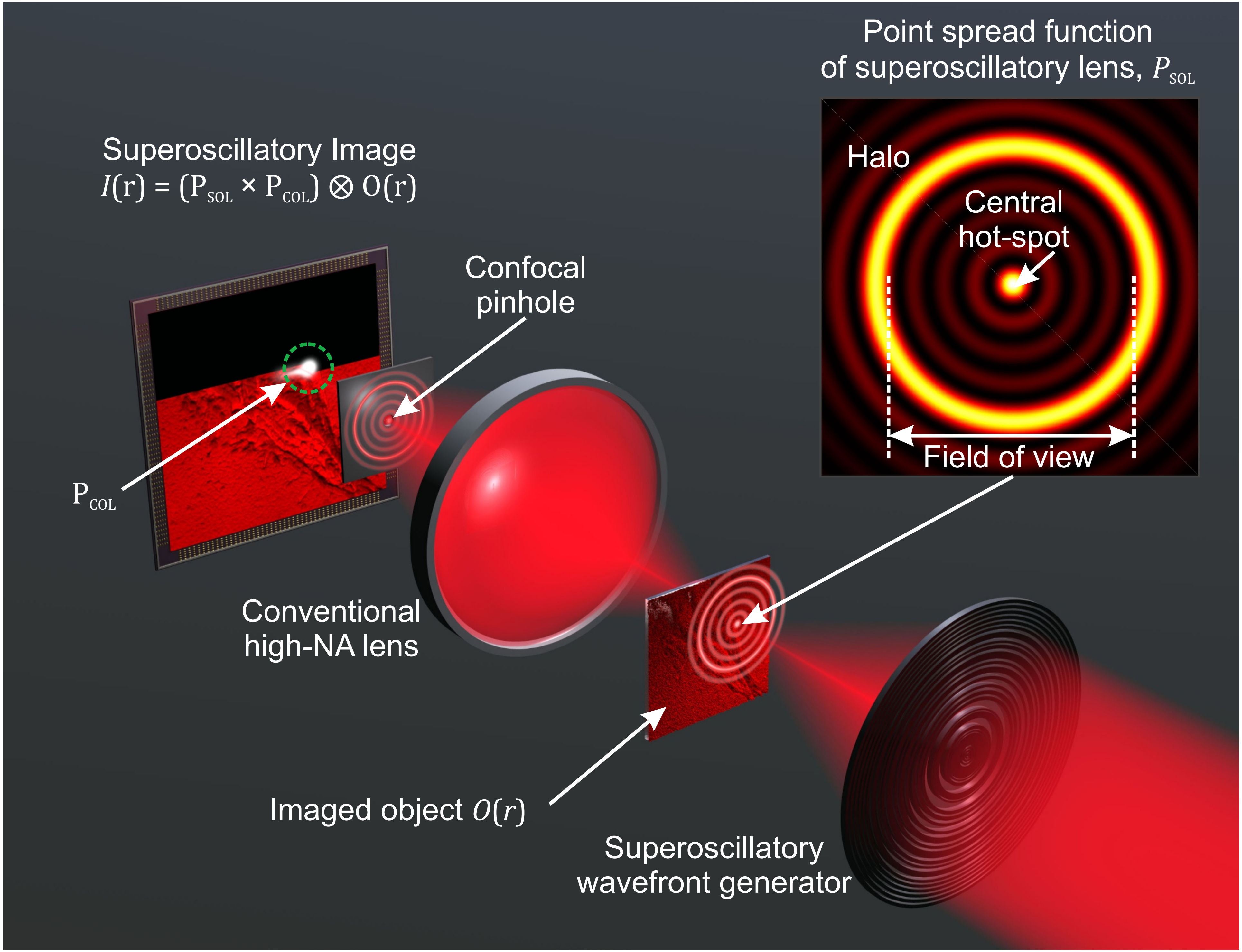
Point spread function of superoscillatory lens, P_{SOL}
Halo
Central hot-spot
Field of view
Superoscillatory Image
$I(r) = (P_{SOL} \times P_{COL}) \otimes O(r)$
Confocal pinhole
P_{COL}
Conventional high-NA lens
Imaged object $O(r)$
Superoscillatory wavefront generator

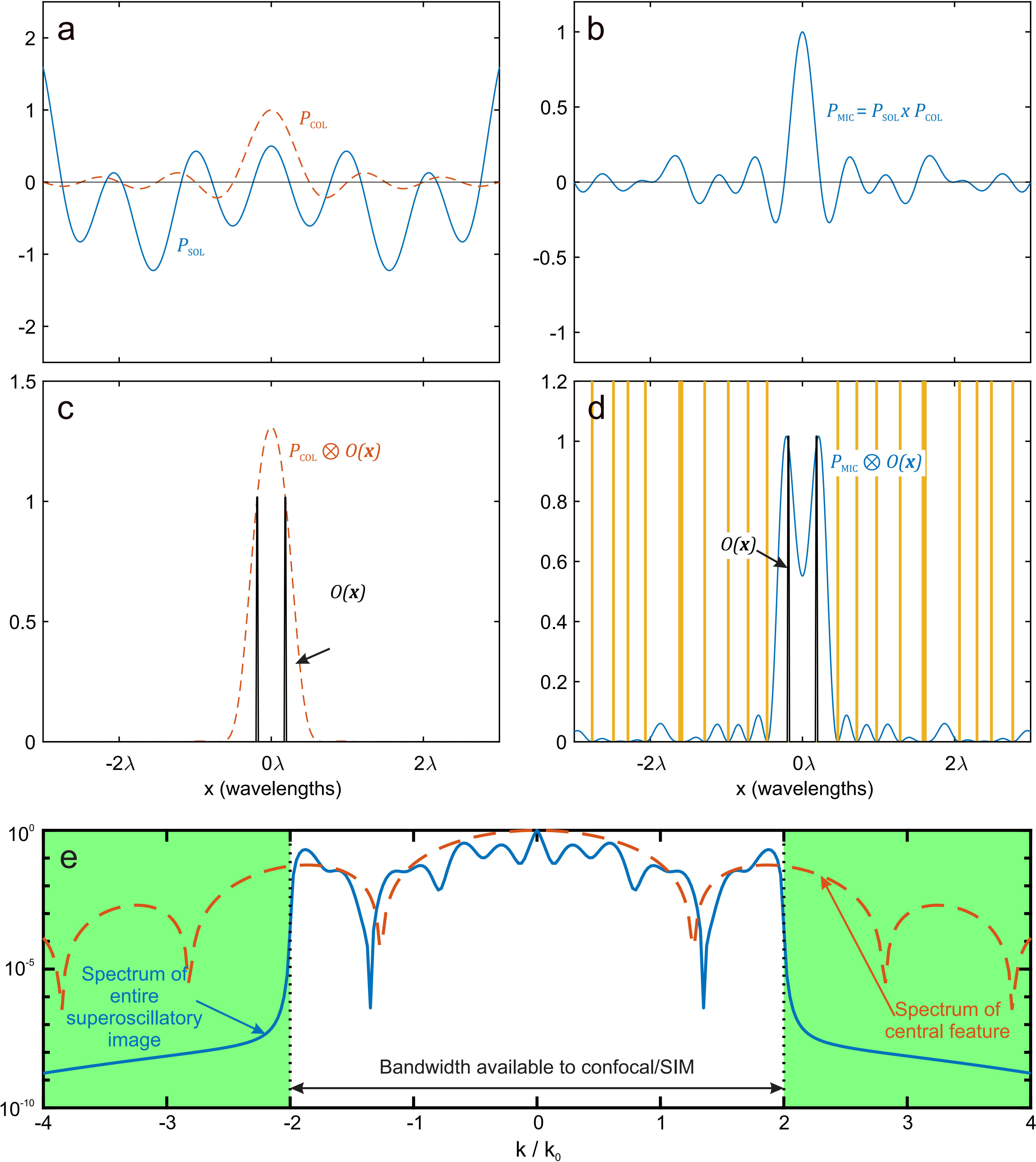
a
b
c
d
e
P_{COL}
P_{SOL}
$P_{MIC} = P_{SOL} x P_{COL}$
$P_{COL} \otimes O(\mathbf{x})$
$O(\mathbf{x})$
$P_{MIC} \otimes O(\mathbf{x})$
$O(\mathbf{x})$
2
1
0
-1
-2
0.5
-0.5
1.5
1.2
0.8
0.6
0.4
0.2
-2λ
0λ
2λ
x (wavelengths)
x (wavelengths)
10^0
10^{-5}
10^{-10}
-4
-3
-2
-1
0
1
2
3
4
k / k_0
Spectrum of entire superoscillatory image
Spectrum of central feature
Bandwidth available to confocal/SIM

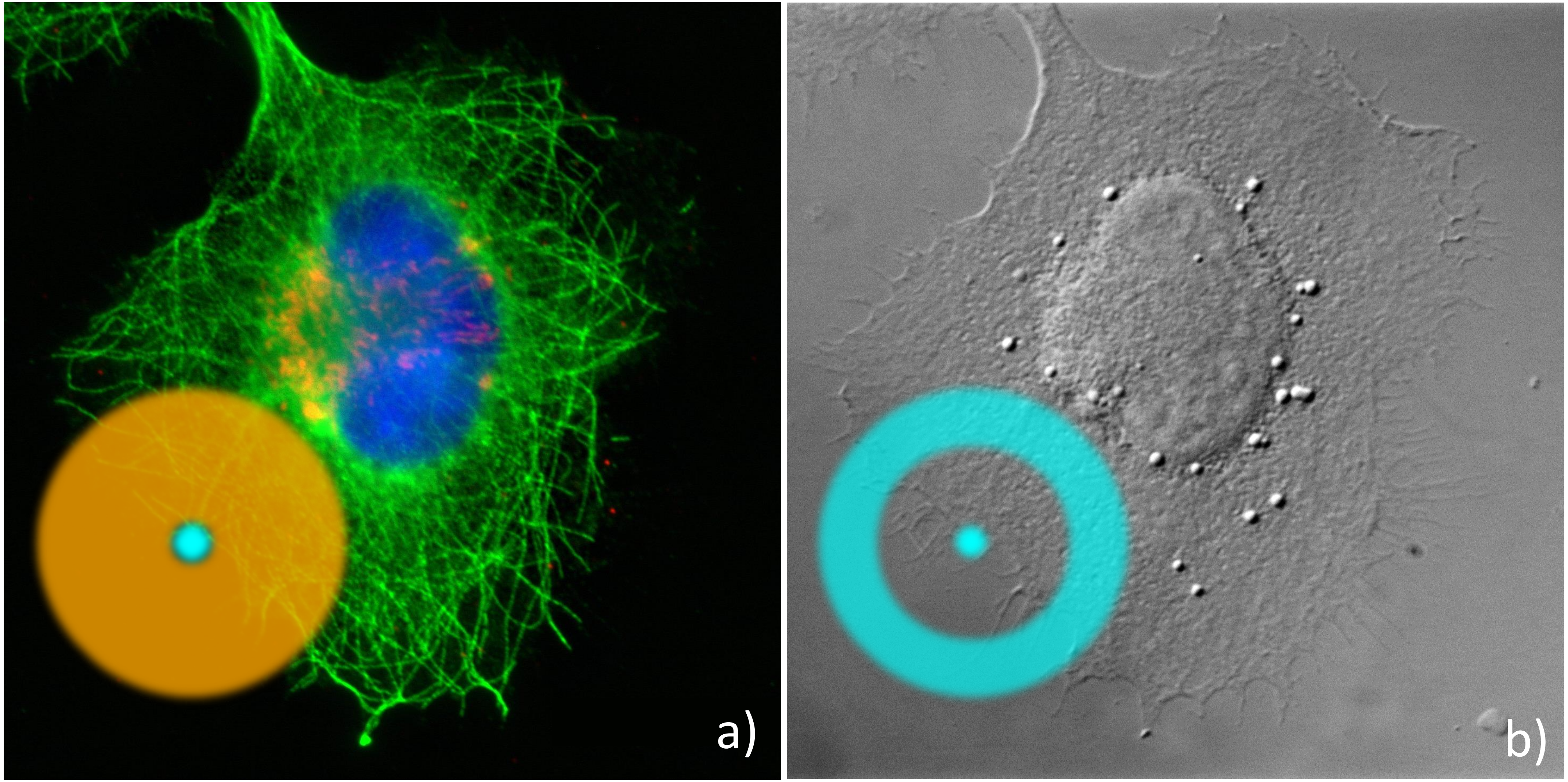
a)
b)

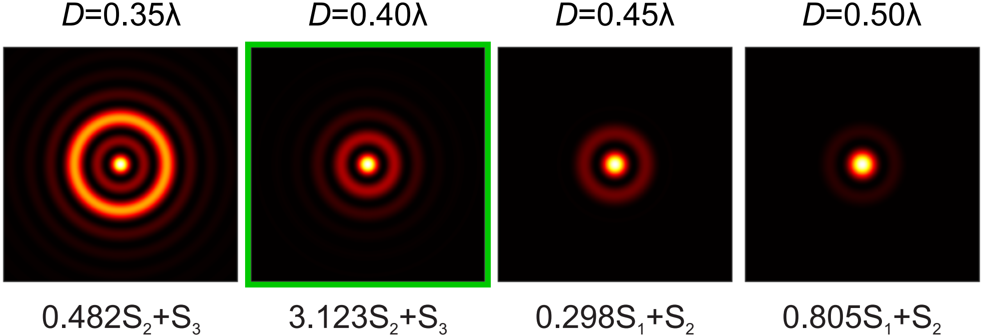

D=0.35λ D=0.40λ D=0.45λ D=0.50λ

$0.482S_2+S_3$ $3.123S_2+S_3$ $0.298S_1+S_2$ $0.805S_1+S_2$

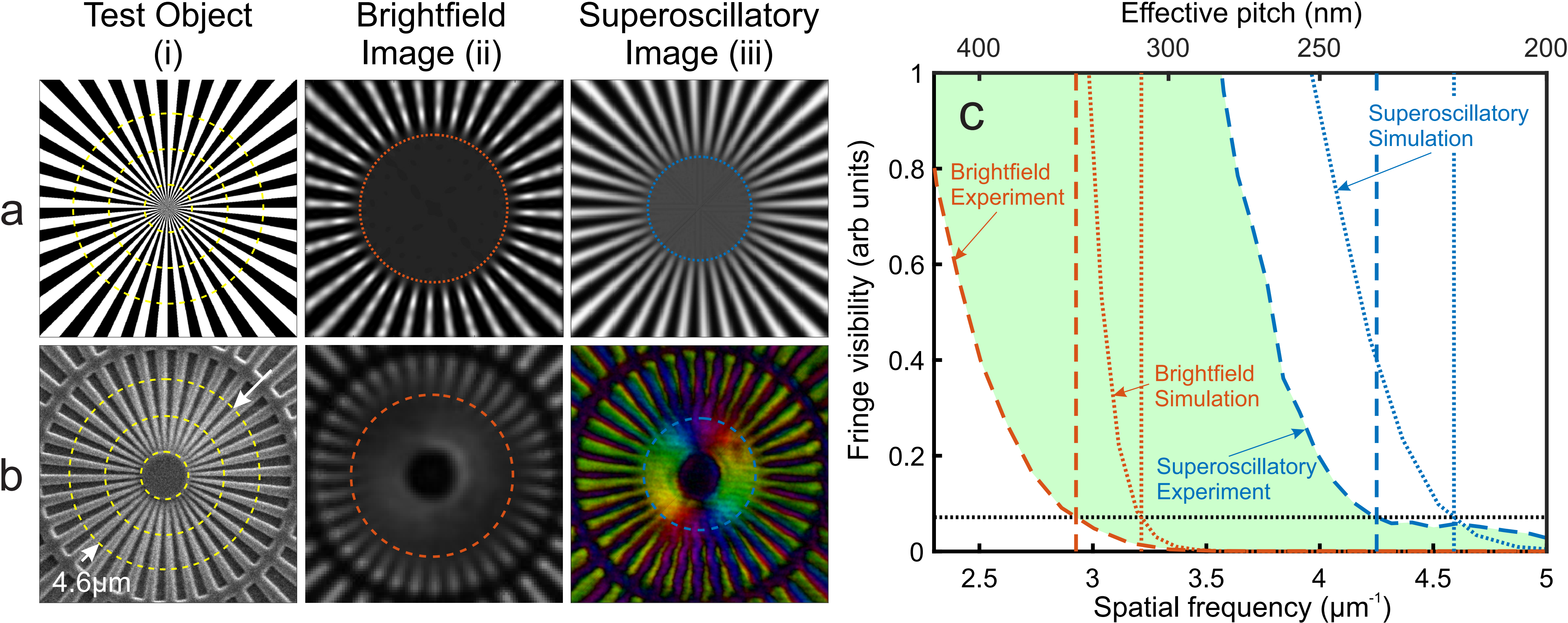
Test Object (i)
Brightfield Image (ii)
Superoscillatory Image (iii)
a
b
4.6μm
Effective pitch (nm)
400
300
250
200
c
Superoscillatory Simulation
Brightfield Experiment
Brightfield Simulation
Superoscillatory Experiment
Fringe visibility (arb units)
1
0.8
0.6
0.4
0.2
0
2.5
3
3.5
4
4.5
5
Spatial frequency (μm^{-1})

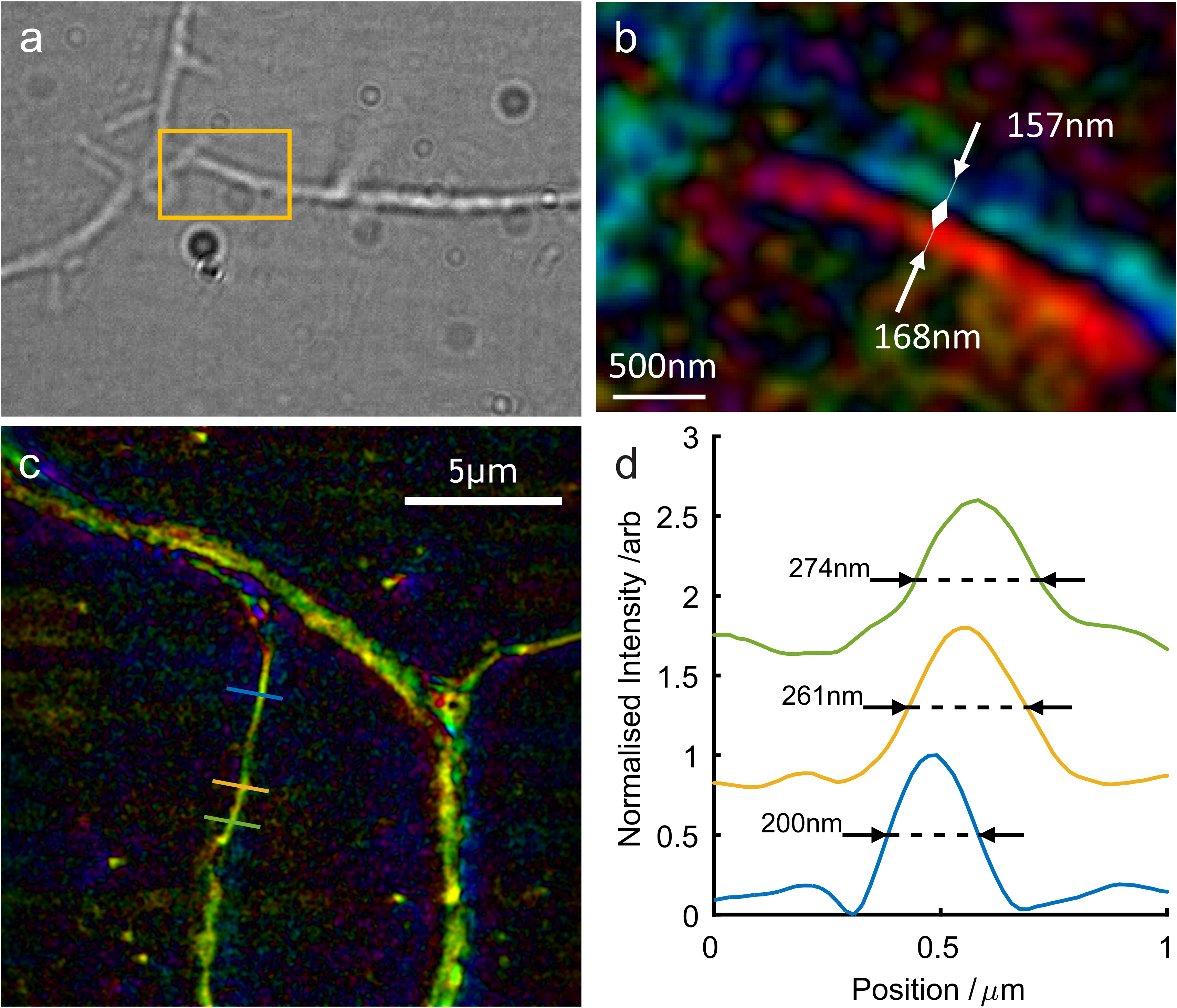
a
b
157nm
168nm
500nm
c
5μm
d
274nm
261nm
200nm
Normalised Intensity /arb
0
0.5
1
1.5
2
2.5
3
0
0.5
1
Position / μm

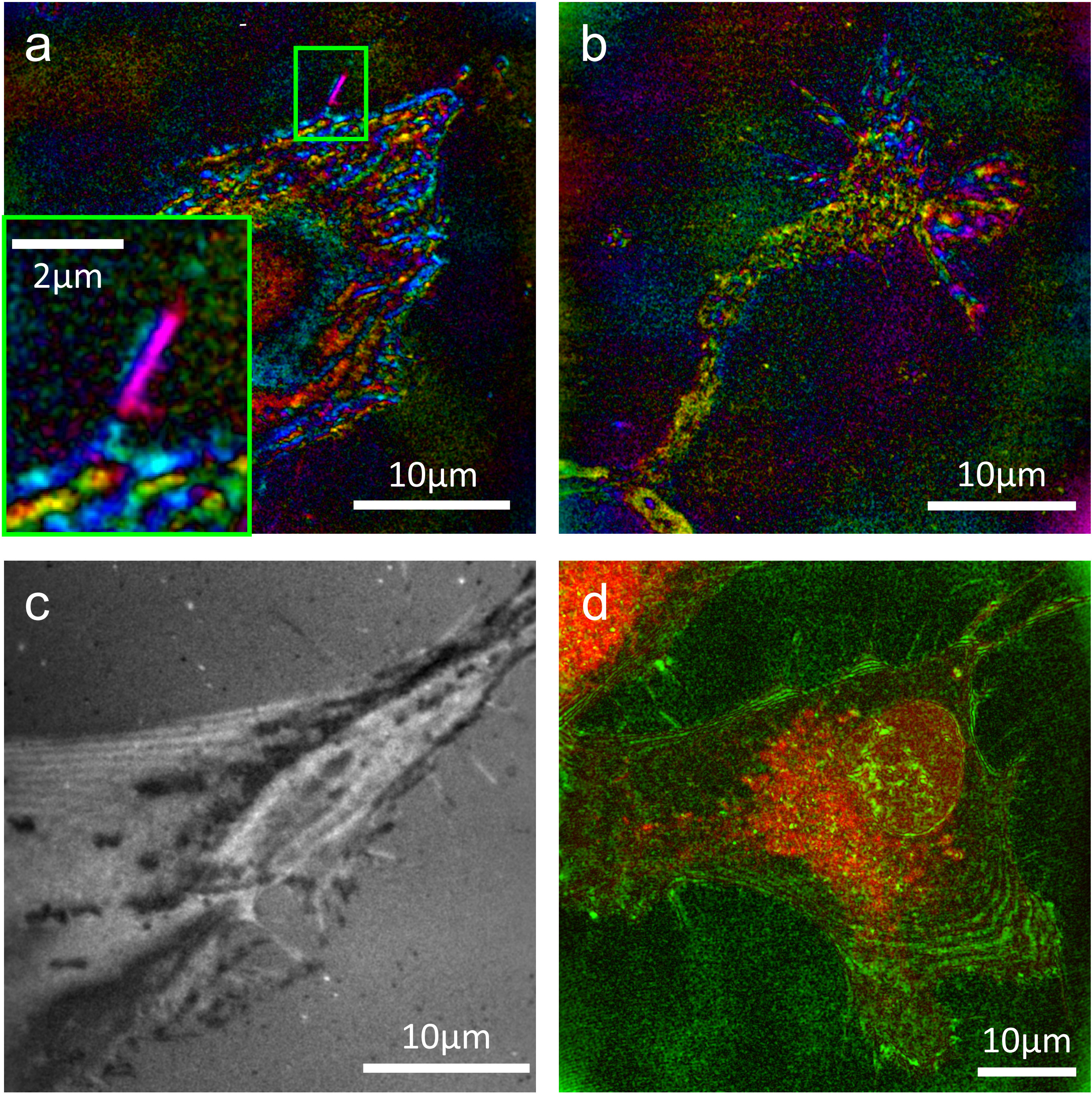
a
2µm
10µm
b
10µm
c
10µm
d
10µm